

A Graphic Approach to Performance Analysis of Multistage Linear Interference Canceller in Long-Code CDMA Systems

Chien-Hwa Hwang, *Student Member, IEEE*, Chang-Su Kim, *Member, IEEE*, and C.-C. Jay Kuo, *Fellow, IEEE*

Abstract—The signal-to-interference-plus-noise-ratio performance of the multistage linear parallel and successive interference cancellers (LPIC and LSIC) in a long-code code-division multiple-access system is analyzed with a graphic approach in this paper. The decision statistic is modeled as a Gaussian random variable, whose mean and variance can be expressed as functions of moments of \mathbf{R} for the LPIC and \mathbf{L} for the LSIC, respectively, where \mathbf{R} is the correlation matrix of signature sequences and \mathbf{L} is the strict lower triangular part of \mathbf{R} . Since the complexity of calculating these moments increases rapidly with the growth of the stage index, a graphical representation of moments is developed to facilitate the computation. Propositions are presented to relate the moment calculation problem to several well-known problems in graph theory, i.e., the coloring, the graph decomposition, the biconnected component finding, and the Euler tour problems. It is shown that the derived analytic results match well with simulation results.

Index Terms—Code-division multiple access (CDMA), linear parallel interference cancellation (LPIC), linear successive interference cancellation (LSIC), multiuser detection.

I. INTRODUCTION

SEVERAL multiuser detection algorithms [1] have been proposed to address the multiple-access interference (MAI) problem and the near-far effect in a direct-sequence code-division multiple-access (DS-CDMA) system in the past decade. Among them, the parallel interference cancellation (PIC) [2] and the successive interference cancellation (SIC) [3] schemes have received much attention recently due to the feasibility of their practical implementation. The basic idea is to adopt a matched-filter bank to estimate transmitted signals of interfering users. The estimated interferences are then subtracted in parallel or serially from the received signal. This procedure can be repeated several times to yield a satisfactory result.

The performance of the multistage linear PIC (LPIC) and SIC (LSIC) detectors in long-code CDMA systems is analyzed

in this paper. The performance analysis of various multistage interference cancellers has been conducted by researchers for long-code and short-code systems [4]–[9]. The analysis carried out in previous work was either under some invalid assumptions [4], [5], [8], or for only one stage of interference cancellation¹ [6], [7], [9]. In the former case, the invalid assumptions include: cancelled interferences from different users are uncorrelated; and cancelled interferences and Gaussian noise are uncorrelated [7]. In the latter case, since the simplifying assumptions were not employed, the signal model became so complex that most previous analysis was performed for one interference cancellation stage. In particular, the formula of the conditional mean of the decision statistic was derived up to the second stage of the PIC receiver in [6]. The conditional variance of the decision statistic was also calculated up to the second stage in [7] for the PIC.

In this paper, the correlation effect among all terms in the received signal is carefully examined via matrix algebra, and the closed-form expressions for the conditional mean and variance of each user's decision statistic in each stage are derived accordingly. The performance of LPIC and LSIC receivers depends on high-order moments of \mathbf{R} and \mathbf{L} , respectively, where \mathbf{R} is the correlation matrix of signature sequences and \mathbf{L} is the strict lower triangular part of \mathbf{R} . In this paper, propositions are presented to relate the moment calculation problem to four well-known problems in graph theory, i.e., the vertex coloring, the Euler tour, the graph decomposition, and the biconnected component finding problems. Consequently, graph theory can be employed to calculate high-order moments of \mathbf{R} and \mathbf{L} to study the performance of LPIC and LSIC receivers. Furthermore, even though the properties of LPIC and LSIC receivers are understood to a certain degree today, our research provides a complete quantitative study of the signal-to-interference-plus-noise ratio (SINR) performance of LPIC and LSIC receivers with an arbitrary number of interference cancellation stages.

The rest of the paper is organized as follows. The system model is presented in Section II. The conditional mean and variance of the decision statistic are derived in Section III. A graphical representation is introduced in Section IV to facilitate calculation of the conditional mean and variance of the decision statistic. A method of computing the chromatic polynomial of a digraph is presented in Section V. In Section VI, we demonstrate the method of computing the expectation of expressions formed by graphs. Simulation results are shown in Section VII, and concluding remarks are given in Section VIII.

¹Note that the first stage of the PIC receiver is a matched-filter bank, so that the first interference cancellation step is conducted at the second stage of the PIC receiver.

Paper approved by L. Rasmussen, the Editor for Iterative Detection, Decoding, and ARQ of the IEEE Communications Society. Manuscript received April 30, 2002; revised November 12, 2002 and April 2, 2003. This work was supported in part by the Integrated Media Systems Center, a National Science Foundation Engineering Research Center, under Cooperative Agreement EEC-9529152, and in part by Northrop Grumman. This paper was presented in part at IEEE ICC'02, New York, NY, April 28–May 2, 2002 and at IEEE Globecom'02, Taipei, Taiwan, November 17–21, 2002.

C.-H. Hwang is with the Institute of Communications Engineering, National Tsing Hua University, Hsinchu, Taiwan, R.O.C. (e-mail: chhwang@ieee.org).

C.-S. Kim is with the Department of Information Engineering, Chinese University of Hong Kong, Shatin, N.T., Hong Kong (e-mail: cskim@ieee.org).

C.-C. J. Kuo is with the Integrated Media Systems Center and the Department of Electrical Engineering, University of Southern California, Los Angeles, CA 90089-2564 USA (e-mail: cckuo@sipi.usc.edu).

Digital Object Identifier 10.1109/TCOMM.2003.819204

II. SYSTEM MODEL

Let us consider a synchronous DS-CDMA system with K users. For the i th user, a binary data symbol, $b_i \in \{+1, -1\}$, with the symbol duration T is spread by the binary random signature rectangular waveform $a_i(t)$ with chip duration T_c , spreading ratio $N = T/T_c$, and the amplitude of $a_i(t)$ equal to $\pm\sqrt{2/T}$. The spread signal is modulated by a carrier and then transmitted over a wireless channel. The received signal at the base station can be expressed as

$$r(t) = \sum_{i=1}^K \sqrt{E_i} b_i a_i(t) \cos(\omega_c t + \theta_i) + n(t)$$

where E_i and θ_i are the received energy per symbol and the random carrier phase of user i , respectively, and $n(t)$ is the additive white Gaussian noise (AWGN) with the single-sided power spectral density N_0 . It is assumed throughout this paper that user k is the user of interest.

Let $Z_{p,k}^{(m)}$ and $Z_{s,k}^{(m)}$ be the decision statistics of the LPIC and LSIC receivers, respectively, of user k at the m th stage. Similarly, we use $\mathbf{z}_p^{(m)}$ and $\mathbf{z}_s^{(m)}$ to denote the decision statistic vectors of the LPIC and LSIC receivers, respectively, at the m th stage, i.e., $\mathbf{z}_x^{(m)} = [Z_{x,1}^{(m)} \cdots Z_{x,K}^{(m)}]^\top$, $x \in \{p, s\}$. The recursive relations of the LPIC and LSIC are given by [10], [11]

$$\mathbf{z}_p^{(m)} = \mathbf{z}_p^{(1)} + (\mathbf{I} - \mathbf{R})\mathbf{z}_p^{(m-1)}, \text{ (LPIC)} \quad (1)$$

and

$$\begin{cases} (\mathbf{I} + \mathbf{L})\mathbf{z}_s^{(1)} = \mathbf{y}, \\ (\mathbf{I} + \mathbf{L})\mathbf{z}_s^{(m)} + \mathbf{L}^\top \mathbf{z}_s^{(m-1)} = \mathbf{y}, m > 1, \end{cases} \text{ (LSIC)} \quad (2)$$

where \mathbf{I} is the identity matrix, $\mathbf{R}_{i,j}$ is equal to $\cos\theta_{i,j}\rho_{i,j}$ with $\theta_{i,j} = \theta_i - \theta_j$ and $\rho_{i,j} \in [-1, 1]$ being the normalized crosscorrelation of $a_i(t)$ and $a_j(t)$, \mathbf{L} is the strict lower triangular part of \mathbf{R} , and the superscript T denotes the matrix transpose operator. The first-stage decision statistic vector $\mathbf{z}_p^{(1)}$ in (1) and \mathbf{y} in (2) are given by

$$\mathbf{z}_p^{(1)} = \mathbf{y} = \mathbf{R}\mathbf{W}\mathbf{b} + \mathbf{n}$$

where $\mathbf{W} = \text{diag}\{\sqrt{E_1} \cdots \sqrt{E_K}\}$, $\mathbf{b} = [b_1 \cdots b_K]^\top$, $\mathbf{n} = [\xi_1 \cdots \xi_K]^\top$, and ξ_i is the AWGN output at the user i 's matched filter.

III. CALCULATION OF CONDITIONAL MEAN AND VARIANCE

By assuming the equal *a priori* probability of b_k , i.e., $\Pr(b_k = 1) = \Pr(b_k = -1) = 0.5$, the output SINR of user k at the m th stage, $\text{SINR}_{x,k}^{(m)}$, $x \in \{p, s\}$, is given by

$$\text{SINR}_{x,k}^{(m)} = \frac{E^2[Z_{x,k}^{(m)}|b_k]}{\text{Var}[Z_{x,k}^{(m)}|b_k]}. \quad (3)$$

The goal of this section is to obtain the conditional mean and variance of decision statistic, i.e., $E[Z_{x,k}^{(m)}|b_k]$ and $\text{Var}[Z_{x,k}^{(m)}|b_k]$, for arbitrary m, k , and $x \in \{p, s\}$.

A. LPIC

The recursion in (1) can be expressed as a one-shot matrix filter

$$\begin{aligned} \mathbf{z}_p^{(m)} &= [\mathbf{I} + (\mathbf{I} - \mathbf{R}) + (\mathbf{I} - \mathbf{R})^2 + \cdots + (\mathbf{I} - \mathbf{R})^{m-1}] \mathbf{z}_p^{(1)} \\ &= \mathbf{F}_p^{(m)} \mathbf{z}_p^{(1)} \end{aligned} \quad (4)$$

where $\mathbf{F}_p^{(m)} = \sum_{i=0}^{m-1} (\mathbf{I} - \mathbf{R})^i = [\mathbf{I} - (\mathbf{I} - \mathbf{R})^m] \mathbf{R}^{-1} = \mathbf{R}^{-1} [\mathbf{I} - (\mathbf{I} - \mathbf{R})^m]$. By (4), we have the conditional mean and variance of $Z_{p,k}^{(m)}$ as shown in (5) at the bottom of the page, where we have

$$\begin{cases} X_{p,k}^{(m)} = E_{\theta,\rho}[(\mathbf{R} - \mathbf{I})^m]_{k,k} \\ Y_{p,k}^{(m)} = E_{\theta,\rho}[(\mathbf{R} - \mathbf{I})^m \mathbf{W}^2 (\mathbf{R} - \mathbf{I})^m]_{k,k}. \end{cases} \quad (6)$$

Since each component of \mathbf{R} is a random variable of signature sequence crosscorrelation and carrier phase difference, $X_{p,k}^{(m)}$ and $Y_{p,k}^{(m)}$ are obtained by averaging over these two random variable sets. Detailed derivations of (5), (6), and the results presented in Section III-B can be found in [12].

B. LSIC

By defining $\mathbf{M} = (\mathbf{I} + \mathbf{L})^{-1} \mathbf{L}^\top$, the recursion in (2) leads to a one-shot matrix filter [11]

$$\mathbf{z}_s^{(m)} = \sum_{i=0}^{m-1} (-\mathbf{M})^i (\mathbf{I} + \mathbf{L})^{-1} \mathbf{y} = \mathbf{F}_s^{(m)} \mathbf{y} \quad (7)$$

where $\mathbf{F}_s^{(m)} = \sum_{i=0}^{m-1} (-\mathbf{M})^i (\mathbf{I} + \mathbf{L})^{-1} = [\mathbf{I} - (-\mathbf{M})^m] \mathbf{R}^{-1}$. From (7), we have (8), as shown at the bottom of the page, where

$$\begin{cases} X_{s,k}^{(m)} = E_{\theta,\rho}[(\mathbf{M}^m)_{k,k}], \\ Y_{s,k}^{(m)} = E_{\theta,\rho}[(\mathbf{M}^m \mathbf{W}^2 \mathbf{N}^m)_{k,k}] \\ V_{s,k}^{(i,m)} = E_{\theta,\rho}[(\mathbf{M}^i (\mathbf{I} + \mathbf{L})^{-1} \mathbf{N}^m)_{k,k}] \end{cases} \quad (9)$$

with $\mathbf{N} = \mathbf{M}^\top$.

$$\begin{cases} E[Z_{p,k}^{(m)}|b_k] = \sqrt{E_k} b_k [1 - (-1)^m X_{p,k}^{(m)}] \\ \text{Var}[Z_{p,k}^{(m)}|b_k] = \left(\frac{N_0}{2}\right) \sum_{i=0}^{m-1} (-1)^i [X_{p,k}^{(i)} - (-1)^m X_{p,k}^{(m+i)}] + Y_{p,k}^{(m)} - \left(\sqrt{E_k} X_{p,k}^{(m)}\right)^2 \end{cases} \quad (5)$$

$$\begin{cases} E[Z_{s,k}^{(m)}|b_k] = \sqrt{E_k} b_k [1 - (-1)^m X_{s,k}^{(m)}] \\ \text{Var}[Z_{s,k}^{(m)}|b_k] = \left(\frac{N_0}{2}\right) \sum_{i=0}^{m-1} (-1)^i [V_{s,k}^{(i,m)} - (-1)^m V_{s,k}^{(i,m)}] + Y_{s,k}^{(m)} - \left(\sqrt{E_k} X_{s,k}^{(m)}\right)^2 \end{cases} \quad (8)$$

As given in (5) and (8), we note that $E[Z_{x,k}^{(m)}|b_k]$ and $\text{Var}[Z_{x,k}^{(m)}|b_k]$, $x \in \{p, s\}$, are determined by the moments of matrices composed by $(\mathbf{R} - \mathbf{I})$, \mathbf{W} , \mathbf{M} , \mathbf{N} , and $(\mathbf{I} + \mathbf{L})^{-1}$ as presented in (6) and (9).

In the following, we use $X_{p,k}^{(m)}$ and $X_{s,k}^{(m)}$ as examples to illustrate our strategy in computing their values. By expanding matrix multiplications, $X_{p,k}^{(m)}$ can be written as

$$\begin{aligned} X_{p,k}^{(m)} &= \sum_{t_1=1}^K \sum_{t_2=1}^K \cdots \sum_{t_{m-1}=1}^K E[(\mathbf{R} - \mathbf{I})_{k,t_1} (\mathbf{R} - \mathbf{I})_{t_1,t_2} \cdots \\ &\quad \times (\mathbf{R} - \mathbf{I})_{t_{m-2},t_{m-1}} (\mathbf{R} - \mathbf{I})_{t_{m-1},k}] \\ &= \sum_{t_1=1}^K \sum_{t_2=1}^K \cdots \sum_{t_{m-1}=1}^K E[\cos \theta_{k,t_1} \cos \theta_{t_1,t_2} \cdots \\ &\quad \times \cos \theta_{t_{m-1},k}] E[\rho_{k,t_1} \rho_{t_1,t_2} \cdots \rho_{t_{m-1},k}]. \quad (10) \end{aligned}$$

Similarly, $X_{s,k}^{(m)}$ can be expressed as

$$\begin{aligned} X_{s,k}^{(m)} &= \sum_{t_1=1}^K \sum_{t_2=1}^K \cdots \sum_{t_{m-1}=1}^K E[\mathbf{M}_{k,t_1} \mathbf{M}_{t_1,t_2} \cdots \\ &\quad \mathbf{M}_{t_{m-2},t_{m-1}} \mathbf{M}_{t_{m-1},k}]. \quad (11) \end{aligned}$$

Since \mathbf{L} is a strict lower triangular matrix, $(\mathbf{I} + \mathbf{L})^{-1} = \sum_{i=0}^{K-1} (-\mathbf{L})^i$ and the (r, s) th element in \mathbf{M} can be given as

$$\begin{aligned} \mathbf{M}_{r,s} &= \sum_{i=0}^{K-1} (-1)^i (\mathbf{L}^i \mathbf{L}^\top)_{r,s} \\ &= \sum_{i=0}^{K-1} (-1)^i \sum_{j_1=1}^K \sum_{j_2=1}^K \cdots \sum_{j_i=1}^K \mathbf{L}_{r,j_1} \mathbf{L}_{j_1,j_2} \cdots \\ &\quad \times \mathbf{L}_{j_{i-1},j_i} \mathbf{L}_{j_i,s}^\top \\ &= \sum_{i=0}^{K-1} (-1)^i \sum_{j_1=1}^K \sum_{j_2=1}^K \cdots \sum_{\substack{j_i=1 \\ j_1 < r \ j_2 < j_1 \\ j_i < j_{i-1} \\ j_i < s}}^K (\rho_{r,j_1} \rho_{j_1,j_2} \cdots \rho_{j_i,s}) \\ &\quad \times (\cos \theta_{r,j_1} \cos \theta_{j_1,j_2} \cdots \cos \theta_{j_i,s}). \quad (12) \end{aligned}$$

By plugging (12) into (11), we obtain the expression of $X_{s,k}^{(m)}$ in terms of $\rho_{i,j}$'s and $\cos \theta_{i,j}$'s.

Thus, we observe that the computation of $X_{p,k}^{(m)}$ requires the grouping of indexes t_i 's according to index values and the calculation of the expected cosine and crosscorrelation terms for each grouping. For $X_{s,k}^{(m)}$, besides grouping of t_i 's and expectation calculations, we need one more step of grouping values for indexes j_l 's, $l \in \{1, \dots, i\}$, according to the inequality constraints imposed at the last equality of (12). These observations also apply to $Y_{x,k}^{(m)}$, $x \in \{p, s\}$ and $V_{s,k}^{(i,m)}$. As the complexity of grouping and expectation calculation grows rapidly with the increase of stage index m and the number of users K , we introduce a graphical representation to facilitate the evaluation of $X_{x,k}^{(m)}$, $Y_{x,k}^{(m)}$, $x \in \{p, s\}$, and $V_{s,k}^{(i,m)}$ in Section IV.

IV. GRAPHICAL APPROACH TO MOMENT CALCULATION

An undirected graph G is a pair of sets denoted by (V, E) , where V is the finite vertex set of G , and its elements are called vertices. E is the edge set of G , and its elements are called edges.

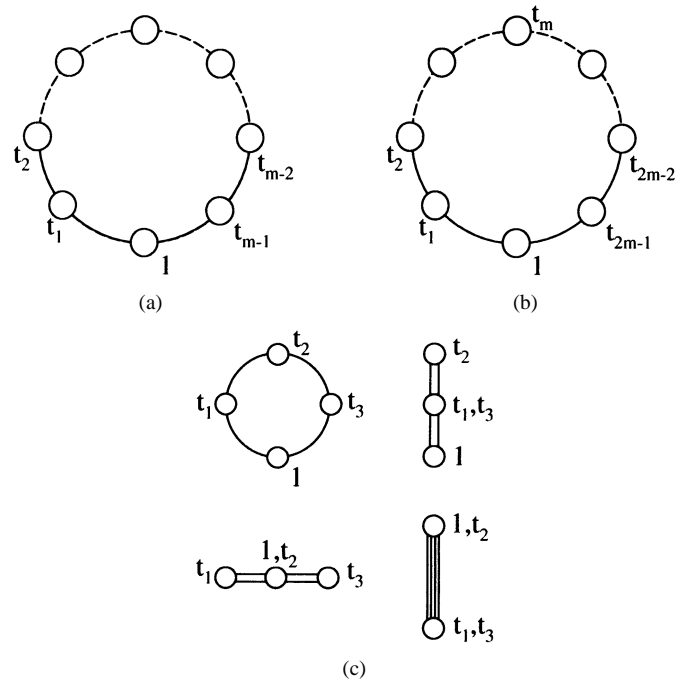


Fig. 1. Graph interpretations of $X_{p,k}^{(m)}$ and $Y_{p,k}^{(m)}$. (a) Graphical representation of $X_{p,k}^{(m)}$. (b) Graphical representation of $Y_{p,k}^{(m)}$. (c) Four evolved graphs of $X_{p,k}^{(4)}$.

An edge with two end vertices u and v is denoted by (u, v) . A directed graph $\vec{G} = (V, A)$ consists of a finite set V of vertices and a set A of ordered pairs of vertices called arcs. An arc from u to v , where $u, v \in V$, is denoted by (u, v) . Examples of undirected and directed graphs are shown in Figs. 1(a) and 2(a), respectively. For definitions of other terminologies in graph theory, we refer to [13].

For simplicity, we use *graph* for an undirected graph and *digraph* for a directed graph throughout the paper. Graphs and digraphs provide excellent tools for the analysis of LPIC and LSIC receivers, respectively, as discussed below.

A. LPIC

The two graphs in Fig. 1(a) and (b) are the graphical representations of $X_{p,k}^{(m)}$ and $Y_{p,k}^{(m)}$, respectively, where except for vertex 1, the remaining vertices, t_1, t_2, \dots , represent summation variables, e.g., in (10) for $X_{p,k}^{(m)}$. Each of them takes an integer from 1 to K , while vertex 1 always takes the integer k (the index of the desired user). Besides, there is a constraint, i.e., adjacent vertices cannot take the same integer. This is the same as the constraint in the coloring problem, e.g., [13], where we attempt to find a mapping $c: V \rightarrow \{1, 2, \dots, K\}$ such that $c(u) \neq c(v)$ for every edge $(u, v) \in E$.

Our task is to determine all possible ways in coloring the graph. This problem can be solved in two steps. The first one, performed by computer search, is to find all possible groupings of vertices such that adjacent vertices are not in the same group. The second step is to draw vertices in one group with the same color such that the color for each group is different. In the current context, we should find out all possible ways of merging nonadjacent vertices in the graphical representation. Then, an integer from 1 to K is assigned to each merged vertex, such that

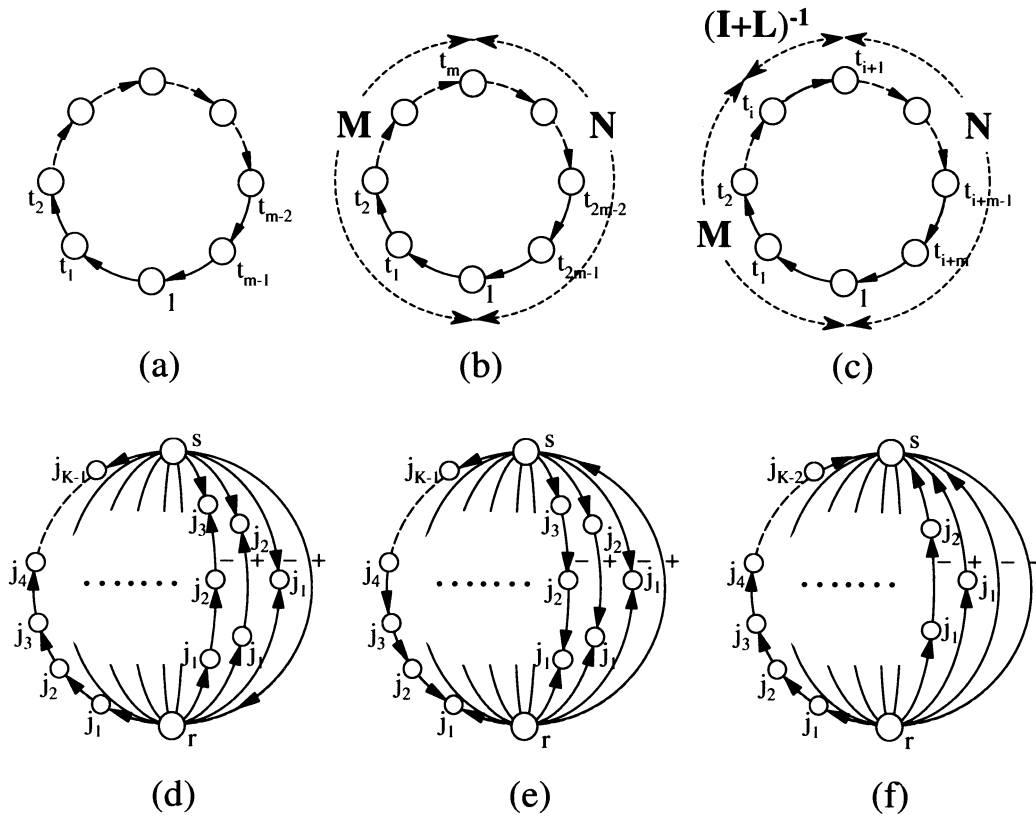


Fig. 2. Graphical representation of $X_{s,k}^{(m)}$, $Y_{s,k}^{(m)}$, and $V_{s,k}^{(i,m)}$. (a)–(c) Macro representations of $X_{s,k}^{(m)}$, $Y_{s,k}^{(m)}$, and $V_{s,k}^{(i,m)}$, respectively. (d)–(f) Detailed representations of the arc (r, s) of the macro representations in (a)–(c), respectively.

the integer for the merged vertex where vertex 1 is located is k , and the assigned integer is different for every merged vertex. A graph, yielded by the mergence of vertices of G , is called an *evolved graph* of G .

Fig. 1(c) shows four possible evolved graphs for $X_{p,k}^{(4)}$ or $Y_{p,k}^{(2)}$. The upper left one corresponds to the case that none of vertices 1, t_1 , t_2 , and t_3 are merged together. Since vertex 1 always takes integer k , the total number of methods in assigning vertices with integers from 1 to K is equal to $(K-1)(K-2)(K-3)$. For the upper right one, vertices t_1 and t_3 are merged, and there are $(K-1)(K-2)$ ways of assigning integers. For the lower left one, vertices 1 and t_2 are merged together, and the total number of assignment is $(K-1)(K-2)$. For the lower right, there are two vertices in the evolved graph, which are merged via pairs (t_1, t_3) and $(1, t_2)$. There are $(K-1)$ possible assignments.

Let $\psi(u)$ denote the integer assigned to vertex u , then $X_{p,k}^{(m)}$ and $Y_{p,k}^{(m)}$ can be obtained by calculating

$$\begin{aligned} & E[\cos \theta_{k,\psi(t_1)} \cos \theta_{\psi(t_1),\psi(t_2)} \cdots \cos \theta_{\psi(t_{m-1}),k}] \\ & E[\rho_{k,\psi(t_1)} \rho_{\psi(t_1),\psi(t_2)} \cdots \rho_{\psi(t_{m-1}),k}] \end{aligned}$$

for each evolved graph G_e of G . Let $E_\theta(G_e)$ and $E_\rho(G_e)$ denote the first and the second expectations, respectively. In Fig. 1(c), $E_\rho(G_e)$ is equal to $E_\rho(G_{e,1}) = E[\rho_{k,\psi(t_1)} \rho_{\psi(t_1),\psi(t_2)} \rho_{\psi(t_2),\psi(t_3)} \rho_{\psi(t_3),k}]$, $E_\rho(G_{e,2}) = E[\rho_{k,\psi(t_1)}^2 \rho_{\psi(t_1),\psi(t_2)}]$, $E_\rho(G_{e,3}) = E[\rho_{k,\psi(t_1)}^2 \rho_{\psi(t_1),\psi(t_3)}]$, and $E_\rho(G_{e,4}) = E[\rho_{k,\psi(t_1)}^4]$ for the upper left, the upper right, the

lower left, and the lower right evolved graphs, respectively. Similarly, $E_\theta(G_e)$ is equal to $E_\theta(G_{e,1}) = E[\cos \theta_{k,\psi(t_1)} \cos \theta_{\psi(t_1),\psi(t_2)} \cos \theta_{\psi(t_2),\psi(t_3)} \cos \theta_{\psi(t_3),k}]$, $E_\theta(G_{e,2}) = E[\cos^2 \theta_{k,\psi(t_1)} \cos^2 \theta_{\psi(t_1),\psi(t_2)}]$, $E_\theta(G_{e,3}) = E[\cos^2 \theta_{k,\psi(t_1)} \cos^2 \theta_{k,\psi(t_3)}]$, and $E_\theta(G_{e,4}) = E[\cos^4 \theta_{k,\psi(t_1)}]$ for evolved graphs in the same order. Then, the value of $X_{p,k}^{(4)}$ is given by

$$\begin{aligned} X_{p,k}^{(4)} &= (K-1)(K-2)(K-3) \cdot E_\rho(G_{e,1})E_\theta(G_{e,1}) \\ &+ (K-1)(K-2) \cdot E_\rho(G_{e,2})E_\theta(G_{e,2}) \\ &+ (K-1)(K-2) \cdot E_\rho(G_{e,3})E_\theta(G_{e,3}) \\ &+ (K-1) \cdot E_\rho(G_{e,4})E_\theta(G_{e,4}). \end{aligned}$$

However, if the current representation G is for $Y_{p,k}^{(m)}$, the computation is somewhat different. As shown in (6), there is an energy matrix \mathbf{W}^2 in the expression of $Y_{p,k}^{(m)}$, which contributes a factor of $E_{\psi(t_m)}$. Therefore, in the computation, we can divide all the evolved graphs into two groups. The first group is for the evolved graphs with vertices 1 and t_m merged together, while the second is for those in which vertices 1 and t_m are not merged. For example, in Fig. 1(c), the two lower graphs belong to the first group, while the two upper ones belong to the second group. The contribution of the evolved graphs from the first group is equal to

$$\begin{aligned} & E_k \cdot (K-1)(K-2) \cdot E_\rho(G_{e,3})E_\theta(G_{e,3}) \\ &+ E_k \cdot (K-1) \cdot E_\rho(G_{e,4})E_\theta(G_{e,4}). \end{aligned}$$

The contribution from the second group is equal to

$$\sum_{\substack{\psi(t_2)=1 \\ \psi(t_2) \neq k}}^K E_{\psi(t_2)} \cdot (K-2)(K-3) \cdot E_{\rho}(G_{e,1}) E_{\theta}(G_{e,1}) \\ + \sum_{\substack{\psi(t_2)=1 \\ \psi(t_2) \neq k}}^K E_{\psi(t_2)} \cdot (K-2) \cdot E_{\rho}(G_{e,2}) E_{\theta}(G_{e,2}).$$

The reason for counting factors $(K-2)(K-3)$ and $(K-2)$ is that vertex 1 is assigned with the fixed integer k , and the integer taken by vertex t_m is a summation variable.

B. LSIC

Digraphs used to interpret $X_{s,k}^{(m)}$, $Y_{s,k}^{(m)}$, and $V_{s,k}^{(i,m)}$ are given in Fig. 2(a)–(c). Identical to the case in LPIC, except for vertex 1, the remaining vertices t_1, t_2, \dots represent the summation variables, e.g., in (11) for $X_{s,k}^{(m)}$. Each of them takes an integer from 1 to K , while vertex 1 always takes the integer k . In Fig. 2(a), arcs represent elements in matrix \mathbf{M} . In Fig. 2(b), arcs $\{(1, t_1), \dots, (t_{m-1}, t_m)\}$ and $\{(t_m, t_{m+1}), \dots, (t_{2m-1}, 1)\}$ represent elements in \mathbf{M} and \mathbf{N} , respectively. In Fig. 2(c), $\{(1, t_1), \dots, (t_{i-1}, t_i)\}$, (t_i, t_{i+1}) , and $\{(t_{i+1}, t_{i+2}), \dots, (t_{i+m}, 1)\}$ are elements in \mathbf{M} , $(\mathbf{I} + \mathbf{L})^{-1}$, and \mathbf{N} , respectively. More specifically, arc (r, s) represents the $(\psi(r), \psi(s))$ th element in the corresponding matrix. The reason that digraphs are used here is because \mathbf{M} , $(\mathbf{I} + \mathbf{L})^{-1}$, and \mathbf{N} are not symmetric matrices.

An arc (r, s) in Fig. 2(a)–(c), signifying elements in \mathbf{M} , \mathbf{N} , and $(\mathbf{I} + \mathbf{L})^{-1}$, can be represented by detailed digraphs in Fig. 2(d) and (e) and a detailed mixed graph in Fig. 2(f), respectively. Fig. 2(f) is a mixed graph since it contains one edge. Let us take Fig. 2(d) as an example. It can be seen from (12) that each path from vertex r to s represents a specific value of i ($0 \leq i \leq K-1$). The rightmost path corresponds to $i = 0$, while the leftmost one corresponds to $i = K-1$. There is a sign associated with each path, which comes from the factor term $(-1)^i$ in (12). Also, the directions of arcs reflect the constraints on the summation variables j_1, j_2, \dots, j_i . Each vertex in Fig. 2(d)–(f) takes an integer from 1 to K . An arc (u, v) in Fig. 2(d)–(f) represents the $(\psi(u), \psi(v))$ th element in \mathbf{L} , which is equal to $\rho_{\psi(u), \psi(v)} \cos \theta_{\psi(u), \psi(v)}$, if $\psi(u) > \psi(v)$, and 0, otherwise. Thus, the direction of arc (u, v) in Fig. 2(d)–(f) indicates that $\psi(u)$ should be larger than $\psi(v)$ to yield a nonzero value for this arc. On the other hand, the edge in Fig. 2(f) represents the identity matrix \mathbf{I} in $(\mathbf{I} + \mathbf{L})^{-1} = \mathbf{I} - \mathbf{L} + \dots + (-\mathbf{L})^{K-1}$. Thus, the edge has value 1, if $\psi(r) = \psi(s)$, and 0, otherwise.

Digraphs in Fig. 2(a)–(c) are called macro representations of $X_{s,k}^{(m)}$, $Y_{s,k}^{(m)}$, and $V_{s,k}^{(i,m)}$, since their arcs represent elements in \mathbf{M} , \mathbf{N} , and $(\mathbf{I} + \mathbf{L})^{-1}$. The complete representations of $X_{s,k}^{(m)}$, $Y_{s,k}^{(m)}$, and $V_{s,k}^{(i,m)}$ can be obtained by replacing each arc of these macro representations with the corresponding detailed digraph or mixed graph in Fig. 2(d)–(f). For each arc (r, s) in a macro representation, there are K paths between vertices r and s in its complete representation. Therefore, if there are n arcs in a

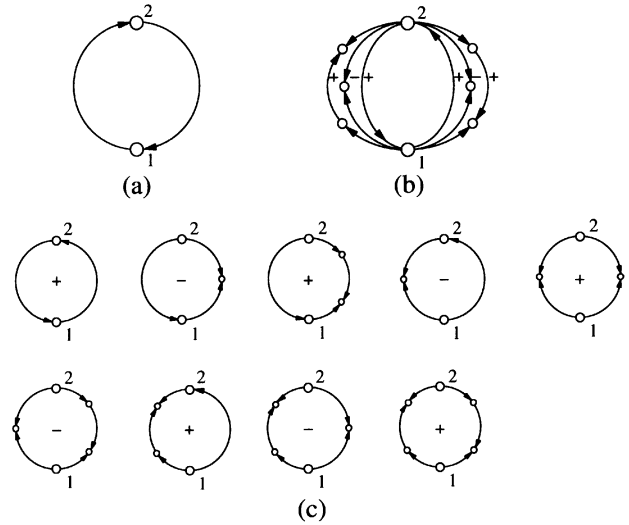


Fig. 3. (a) Macro representation of $X_{s,k}^{(2)}$. (b) Complete representation of (a) when $K = 3$. (c) Nine subrepresentations of (b).

macro representation, the complete representation is equivalent to the summation of K^n subgraphs, which have only one path between each (r, s) . These K^n subgraphs are called subrepresentations. Each subrepresentation has a sign associated with it, which is the multiplicity of the signs of paths within it. Fig. 3 shows examples of the macro representation, the complete representation, and subrepresentations. Fig. 3(a) is the macro representation of $X_{s,k}^{(2)}$. Fig. 3(b) is the complete representation when $K = 3$, obtained by replacing two arcs in Fig. 3(a) with the digraph in Fig. 2(d). Fig. 3(c) shows $K^n = 3^2$ subrepresentations of Fig. 3(b) with the signs indicated at the center.

The values of $X_{s,k}^{(m)}$, $Y_{s,k}^{(m)}$, and $V_{s,k}^{(i,m)}$ can be obtained by summing up the contribution of all subrepresentations. The contribution of a subrepresentation can be computed via the following steps.

- Step 1) Find out all possible ways of vertex mergence in the subrepresentation under the constraint that the two end vertices of an arc should *not* be merged together and the two end vertices of an edge should be merged together.² Note that an edge is degenerated to a vertex after mergence, i.e., there is no self loop. Each digraph yielded by vertex mergence is called an evolved digraph³ of the subrepresentation.
- Step 2) Evaluate $E_{\theta}(G_{e,i})$ and $E_{\rho}(G_{e,i})$ formed by the underlying graph $G_{e,i}$ of each evolved digraph $\vec{G}_{e,i}$.
- Step 3) Let $\{\vec{G}_{e,1,1}, \vec{G}_{e,1,2}, \dots, \vec{G}_{e,1,n_1}\}$ and $\{\vec{G}_{e,2,1}, \vec{G}_{e,2,2}, \dots, \vec{G}_{e,2,n_2}\}$ denote the set of evolved digraphs of the subrepresentation with vertices 1 and t_m of the macro representation being merged and not being merged, respectively. For $\vec{G}_{e,1,i}$'s, compute the total number of valid integer assignments $P(\vec{G}_{e,1,i}, K, [k \rightarrow v_1])$ of $\vec{G}_{e,1,i}$ with the following rule: except that

²An arc (u, v) is equal to zero if $\psi(u) = \psi(v)$, and an edge (u, v) is equal to zero if $\psi(u) \neq \psi(v)$.

³Since vertices connected by edges are merged together, there are no edges after vertex mergence.

the vertex corresponding to vertex 1 (and t_m) of the macro representation is assigned with the integer k , assign each vertex a unique integer i , where $\{1 \leq i \leq K, i \neq k\}$ such that $\psi(u) > \psi(v)$ if there exists an arc from vertex u to v . For $\vec{G}_{e,2,i}$'s, compute the total number of valid integer assignments of $\vec{G}_{e,2,i}$, $P(\vec{G}_{e,2,i}, K, [k \rightarrow v_1], [\psi(t_m) \rightarrow v_{t_m}])$, for each $\psi(t_m) \in \{1, \dots, K\} \setminus k$ with the same rule as above, except that both vertices 1 and t_m of the macro representation are assigned with the integers k and $\psi(t_m)$, respectively.

Step 4) The contribution of the subrepresentation is given by

$$c \cdot \left(\sum_{i=1}^{n_1} \zeta_k \cdot P(\vec{G}_{e,1,i}, K, [k \rightarrow v_1]) E_\rho(G_{e,1,i}) E_\theta(G_{e,1,i}) \right. \\ \left. + \sum_{i=1}^{n_2} \sum_{\substack{\psi(t_m)=1 \\ \psi(t_m) \neq k}}^K \zeta_{\psi(t_m)} \cdot P(\vec{G}_{e,2,i}, K, [k \rightarrow v_1], \right. \\ \left. [\psi(t_m) \rightarrow v_{t_m}]) E_\rho(G_{e,2,i}) E_\theta(G_{e,2,i}) \right) \quad (13)$$

where c is the sign associated with the subrepresentation, $(\zeta_k, \zeta_{\psi(t_m)}) = (1, 1)$ if the current subrepresentation is for $X_{s,k}^{(m)}$ or $V_{s,k}^{(i,m)}$, and $(\zeta_k, \zeta_{\psi(t_m)}) = (E_k, E_{\psi(t_m)})$ if the subrepresentation is for $Y_{s,k}^{(m)}$.

Note that $P(\vec{G}_{e,1,i}, K, [k \rightarrow v_1])$ and $P(\vec{G}_{e,2,i}, K, [k \rightarrow v_1], [\psi(t_m) \rightarrow v_{t_m}])$ in Step 3 above are different from the computation in the LPIC case, where we dealt with the undirected evolved graphs whose vertex was assigned an integer different from those of all others. On the other hand, in the current context, the integer assigned to a vertex should not only be distinct, but also satisfy the constraints given by arc directions. The calculation of valid integer assignment is equivalent to finding the chromatic polynomial of a digraph, where the coloring problem for a digraph $\vec{G} = (V, A)$ is defined to be $f: V \rightarrow \{1, 2, \dots, K\}$ such that $f(u) > f(v)$ for every arc $(u, v) \in A$. In Section V, we introduce an approach for computing the chromatic polynomial of any digraph.

V. CHROMATIC POLYNOMIAL OF A DIGRAPH

The chromatic polynomial of a digraph or mixed graph was discussed in the literature, e.g., [14] and [15], with various definitions of coloring problems. Here, we propose an approach suitable for our application. Before describing the computation of the chromatic polynomial of an arbitrary digraph, let us start with a specific type of digraphs: forests composed of directed trees. A directed tree (or ditree) is a connected acyclic digraph with each vertex having in degree, at most, one. The root of a ditree is the vertex with in degree equal to zero. For simplicity, unless otherwise stated, a forest indicates a forest composed of ditrees below. Also, a ditree is considered as a forest with one component.

Definition 1: Assume that there are n ditrees, $\vec{G}_1, \vec{G}_2, \dots, \vec{G}_n$, from left to right in a forest \vec{G} . The right siblings of a nonroot vertex v are vertices that share the same

parent vertex with v and lie in the right side of v . The right siblings of the root vertex of \vec{G}_i are defined as the root vertices of \vec{G}_j 's ($i < j \leq n$). The descendant number of a vertex is the number of descendants⁴ of the vertex. The right-sum descendant number of a vertex is the sum of the descendant numbers of the vertex itself and its right siblings.

Proposition 1: Let $\epsilon(u)$ and $\Upsilon(u)$ denote the descendant number and the right-sum descendant number of a vertex u , respectively. Also, let $P(\vec{G}, K)$ ⁵ denote the chromatic polynomial, which represents the number of coloring methods for a forest G using K colors with the following two constraints: each vertex u should be assigned with a distinct color or integer $\psi(u) \in [1, K]$; and $\psi(u)$ should be larger than $\psi(v)$ if there exists an arc (u, v) in \vec{G} . Then, $P(\vec{G}, K)$ is given by

$$P(\vec{G}, K) = \binom{K}{\mathcal{N}_v} \prod_{u \in \vec{G}} \binom{\Upsilon(u)}{\epsilon(u)} \quad (14)$$

where \mathcal{N}_v is the number of vertices in \vec{G} .

Proof: Let us assume that there are n ditrees $\vec{G}_1, \dots, \vec{G}_n$ from left to right in the forest \vec{G} . Since there are \mathcal{N}_v vertices, we first select \mathcal{N}_v colors from K colors, which has $\binom{K}{\mathcal{N}_v}$ methods. Let r_i denote the root of \vec{G}_i . We divide \mathcal{N}_v colors into n ditrees such that \vec{G}_i is given $\epsilon(r_i)$ colors. Note that $\epsilon(r_i)$ is equal to the number of vertices in \vec{G}_i . There are

$$\prod_{i=1}^n \binom{\sum_{j=i}^n \epsilon(r_j)}{\epsilon(r_i)} = \prod_{i=1}^n \binom{\Upsilon(r_i)}{\epsilon(r_i)}$$

methods for the division. Then, for ditree \vec{G}_i , the root vertex r_i is assigned with the largest color or integer among the $\epsilon(r_i)$ colors to satisfy the second constraint on the coloring method. If root vertex r_i has k children v_1, \dots, v_k from left to right, the remaining $\epsilon(r_i) - 1$ colors are further divided into k groups with the number of colors in the j th group equal to $\epsilon(v_j)$, which yields $\prod_{j=1}^k \binom{\Upsilon(v_j)}{\epsilon(v_j)}$ methods. Then, in each group, the largest color is assigned to the highest vertex v_j . Similarly, all vertices in the forest can be colored by recursive application of the division and the assignment of the largest color. Therefore, the number of coloring methods for the forest is given by (14). ■

As shown in these examples, it is easy to obtain the chromatic polynomial of a forest. The following proposition, which is a generalization of Birkhoff's Reduction Theorem (see, e.g., [13]), enables us to obtain the chromatic polynomial of any digraph by decomposing the digraph into several forests.

Proposition 2: Let \bar{a}_i be the arc obtained by inverting the direction of arc a_i , $\vec{G} - a_i$ be the digraph obtained by removing a_i from a digraph \vec{G} , and $\vec{G} - a_i + \bar{a}_i$ be the digraph obtained by inverting the direction of a_i in \vec{G} . Then, we have

$$P(\vec{G}, K) = P(\vec{G} - a_i, K) - P(\vec{G} - a_i + \bar{a}_i, K).$$

Proof: Let $a_i = (u, v)$. The coloring for \vec{G} has the constraint that $\psi(u) > \psi(v)$. For $\vec{G} - a_i$, both $\psi(u) > \psi(v)$

⁴A vertex is a descendant of itself.

⁵Unlike $P(\vec{G}, K, [k \rightarrow v_1])$ and $P(\vec{G}, K, [k \rightarrow 1], [\psi(t_m) \rightarrow v_{t_m}])$ having one and two vertices being assigned with predetermined integers, respectively, in the calculation of $P(\vec{G}, K)$, none of the vertex in \vec{G} is specified with a fixed integer.

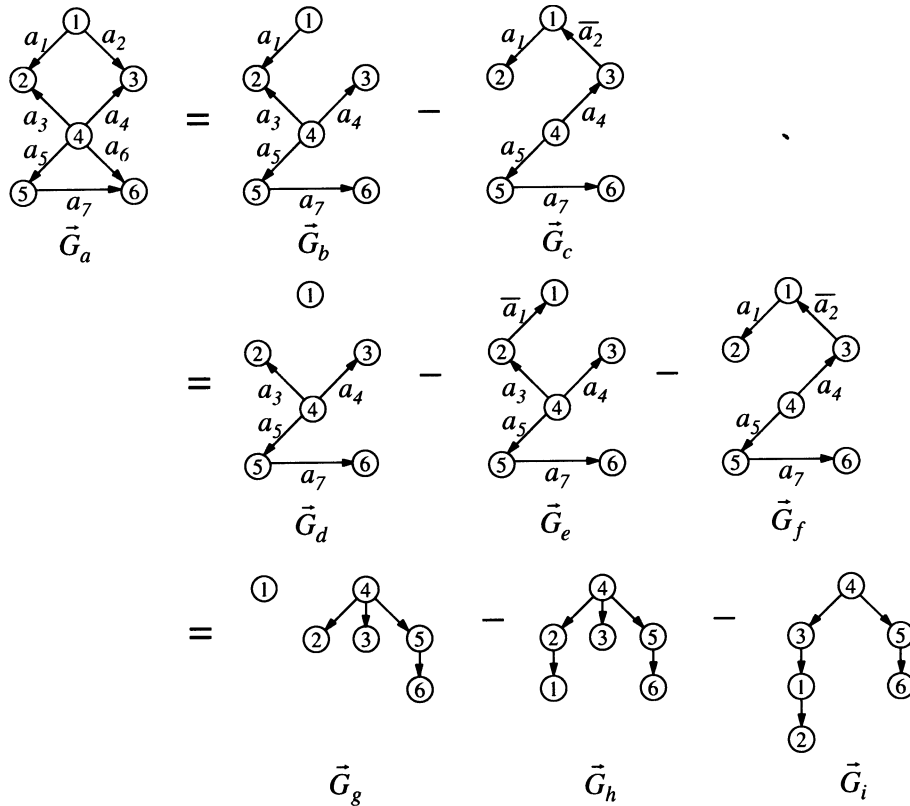


Fig. 4. Illustration of successive application of Proposition 2, where $\vec{G}_g, \vec{G}_h, \vec{G}_i$ are equivalent to $\vec{G}_d, \vec{G}_e, \vec{G}_f$, respectively.

and $\psi(u) < \psi(v)$ are allowed. For $\vec{G} - a_i + \bar{a}_i$, the constraint is $\psi(u) < \psi(v)$. As a result, we obtain $P(\vec{G}, K) = P(\vec{G} - a_i, K) - P(\vec{G} - a_i + \bar{a}_i, K)$. ■

Fig. 4 shows the application of Proposition 2 to decomposing a digraph into forests. By applying Proposition 2 to a_2 in the digraph \vec{G}_a , the chromatic polynomial $P(\vec{G}_a, K)$ is given by $P(\vec{G}_b, K) - P(\vec{G}_c, K)$. Note that arc a_6 is removed in \vec{G}_b and \vec{G}_c , since the inequality relations imposed by a_5 and a_7 make a_6 redundant in the computation of the chromatic polynomial. Also, a_3 of \vec{G}_c is removed because of a_1, \bar{a}_2 , and a_4 . Since \vec{G}_b is still not a forest, Proposition 2 is applied again to decompose \vec{G}_b into two forests \vec{G}_d and \vec{G}_e . Consequently, we have $P(\vec{G}_a, K) = P(\vec{G}_d, K) - P(\vec{G}_e, K) - P(\vec{G}_f, K)$. It is given by $(72 - 30 - 10) \cdot \binom{K}{6} = 32 \cdot \binom{K}{6}$.

The decomposition procedure in Fig. 4 can be represented with sequence notations by $\vec{G}_a \Rightarrow (\vec{G}_b, \vec{G}_c) \Rightarrow (\vec{G}_d, \vec{G}_e, \vec{G}_f)$. A sequence whose element is a forest or a digraph containing a directed cycle is called a *reduced sequence*. Note that we need not decompose a digraph containing a directed cycle, since its chromatic polynomial is 0. By [12], any digraph can be decomposed into a finite reduced sequence by applying Proposition 2 successively.

As shown in (13), we have to consider the chromatic polynomials of digraphs with one or two of the vertices assigned with fixed integers. The chromatic polynomial of a digraph is called the constrained- n chromatic polynomial, if there are n fixed assigned values. To obtain the constrained- n chromatic polynomial, Proposition 2 can be employed iteratively to make vertices with fixed colors the root vertices, and apply the following corollary.

Corollary 1: Let \vec{G} be a forest composed of p ditrees $\vec{G}_1, \dots, \vec{G}_p$ with roots r_1, \dots, r_p . The first n roots r_1, \dots, r_n ($n \leq p$) are already assigned with colors $\psi(r_1), \dots, \psi(r_n)$ such that $\psi(r_1) < \dots < \psi(r_n)$. If there are K available colors, then the number of coloring methods for \vec{G} under this constraint, called the constrained- n chromatic polynomial of \vec{G} , is given by

$$P\left(\bigcup_{i=n+1}^p \vec{G}_i, K - \sum_{i=1}^n \epsilon(r_i)\right) \times \prod_{i=1}^n P\left(\vec{G}_i - r_i, \psi(r_i) - 1 - \sum_{j=1}^{i-1} \epsilon(r_j)\right) \quad (15)$$

where $P(\vec{H}, K)$ is the chromatic polynomial of digraph \vec{H} using K colors, and $\epsilon(r_i)$ is the descendant number of r_i .

Proof: For $1 \leq i \leq n$, the number of available colors for $\vec{G}_i - r_i$ is $\psi(r_i) - 1 - \sum_{j=1}^{i-1} \epsilon(r_j)$. As a result, the total number of coloring methods for \vec{G}_i 's is $\prod_{i=1}^n P(\vec{G}_i - r_i, \psi(r_i) - 1 - \sum_{j=1}^{i-1} \epsilon(r_j))$. For \vec{G}_i 's, $n+1 \leq i \leq p$, the total number of coloring methods is $P(\bigcup_{i=n+1}^p \vec{G}_i, K - \sum_{i=1}^n \epsilon(r_i))$. Hence, the constrained- n chromatic polynomial of \vec{G} is given by (15). ■

VI. COMPUTATION OF EXPECTATIONS ON GRAPHS

As shown in Section V, we require the computation of $E_\theta(\cdot)$ and $E_\rho(\cdot)$ to obtain the matrix moments. In this section, we introduce an approach for computing $E_\theta(\cdot)$ and $E_\rho(\cdot)$ based on some well-known problems in graph theory. Several definitions

and propositions are presented below to facilitate the evaluation of $E_\theta(G_e)$ and $E_\rho(G_e)$. For simplicity, we use G to represent G_e in the following discussion.

Definition 2: An Euler tour of a connected, undirected graph G is a cycle that traverses each edge of G exactly once. Let us denote the number of vertices and edges in G by \mathcal{N}_v and \mathcal{N}_e , respectively. Vertices in G are labeled from 1 to \mathcal{N}_v , and edges are labeled from 1 to \mathcal{N}_e . The Euler tour vector corresponding to an Euler tour is a vector \mathbf{t} , where $t(i) = 0$ if the i th edge is traversed from a lower-label vertex to a higher-label vertex, and $t(i) = 1$, otherwise. Two Euler tours are said to be equivalent if their Euler tour vectors are the same.

It is obvious that the simple cycle in Fig. 1(a) has two Euler tours. Furthermore, the evolved graphs of a simple cycle have at least two Euler tours.

Proposition 3: If there are t_E distinct Euler tours for G , then $E_\theta(G) = t_E/2^{\mathcal{N}_e}$.

Proof: Let $\theta_{i,1}$ and $\theta_{i,2}$ denote the random carrier phases associated with the lower-label and the higher-label vertices connected by the i th edge of G , respectively. Then $E_\theta(G)$ can be written as

$$\begin{aligned} E_\theta(G) &= \mathbb{E} \left[\prod_{i=1}^{\mathcal{N}_e} \cos(\theta_{i,1} - \theta_{i,2}) \right] \\ &= \frac{1}{2^{\mathcal{N}_e}} \cdot \mathbb{E} \left[\prod_{i=1}^{\mathcal{N}_e} \sum_{t_i=0}^1 \exp(j(-1)^{t_i}(\theta_{i,1} - \theta_{i,2})) \right] \\ &= \frac{1}{2^{\mathcal{N}_e}} \cdot \sum_{t_1=0}^1 \sum_{t_2=0}^1 \cdots \sum_{t_{\mathcal{N}_e}=0}^1 \\ &\quad \times \mathbb{E} \left[\exp \left(j \sum_{i=1}^{\mathcal{N}_e} (-1)^{t_i} (\theta_{i,1} - \theta_{i,2}) \right) \right]. \quad (16) \end{aligned}$$

We have $\sum_{i=1}^{\mathcal{N}_e} (-1)^{t_i} (\theta_{i,1} - \theta_{i,2}) = 0$ if and only if $\mathbf{t} = (t_1, t_2, \dots, t_{\mathcal{N}_e})$ forms an Euler tour. Thus, if there are t_E distinct Euler tours for G , $E_\theta(G) = t_E/2^{\mathcal{N}_e}$. ■

Definition 3: A graph $G = (V, E)$ is said to be decomposed into p subgraphs $G_1 = (V_1, E_1)$, $G_2 = (V_2, E_2)$, \dots , $G_p = (V_p, E_p)$, if $\bigcup_{i=1}^p E_i = E$, and $E_i \cap E_j = \emptyset$ for $i \neq j$, and $V_i = \{v \in V: \text{vis one of two vertices of an edge } e \in E_i\}$ for $i = 1, \dots, p$. An even decomposition is a decomposition such that the number of edges incident on each vertex of each subgraph is an even number. The supergraph for the decomposition of G is a graph formed by replacing each subgraph G_i ($1 \leq i \leq p$) with a vertex. Two vertices in the supergraph are connected by an edge, if the corresponding two subgraphs are connected in G . Subgraphs G_i and G_j of G are said to be connected in G if they share at least one vertex in G .

Fig. 5(b) shows examples of the graph decomposition. Let us assume the upper left one to be the original. Then, there are four even decompositions, including the original graph itself. The corresponding supergraphs are shown in Fig. 5(c).

Proposition 4: If there are q even decompositions for a graph G , and S_k denotes the supergraph for the k th even decomposition, then, we have $E_\rho(G) = (1/N^{\mathcal{N}_e}) \sum_{k=1}^q P(S_k, N)$, where $P(S_k, N)$ is the number of coloring methods for S_k with N colors (which corresponds to the spreading ratio) such that adjacent vertices in S_k have different colors.

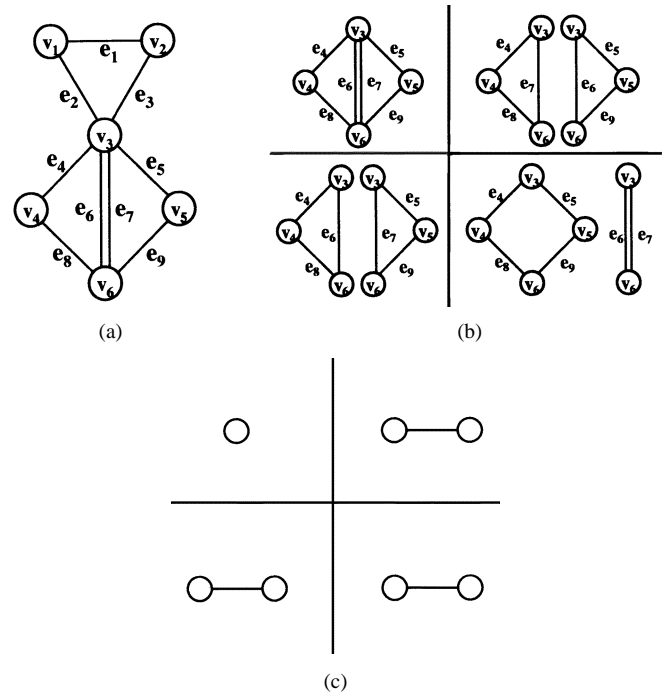


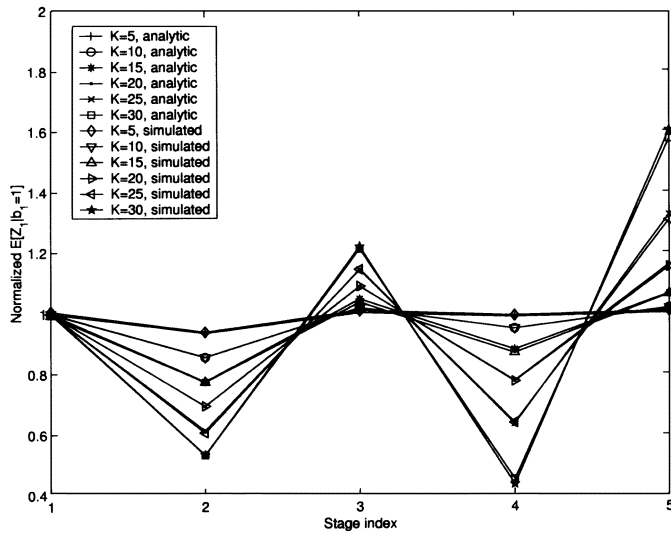
Fig. 5. (a) A graph G . (b) All the even decompositions for the lower subgraph of G in (a). (c) Supergraphs for the four even decompositions in (b).

Proof: Let $c_{i,1}(n)$ and $c_{i,2}(n)$ denote the signature sequences of the lower- and the higher-label vertices of the i th edge in G , respectively. If the lower- or the higher-label vertex of the i th edge is the j th vertex in G , its signature sequence is denoted also by $\alpha_j(n)$. Then, $E_\rho(G)$ is given by

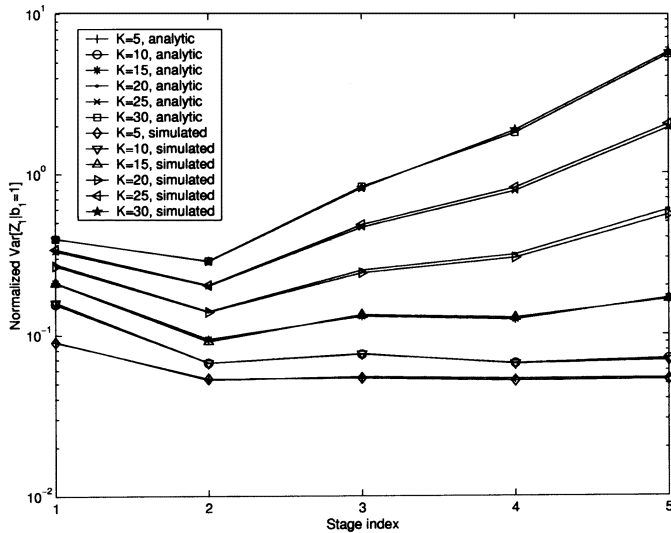
$$\begin{aligned} E_\rho(G) &= \mathbb{E} \left[\prod_{i=1}^{\mathcal{N}_e} \left(\frac{1}{N} \sum_{n_i=1}^N c_{i,1}(n_i) c_{i,2}(n_i) \right) \right] \\ &= \frac{1}{N^{\mathcal{N}_e}} \sum_{n_1=1}^N \cdots \sum_{n_{\mathcal{N}_e}=1}^N \mathbb{E} \left[\prod_{i=1}^{\mathcal{N}_e} c_{i,1}(n_i) c_{i,2}(n_i) \right] \\ &= \frac{1}{N^{\mathcal{N}_e}} \sum_{n_1=1}^N \cdots \sum_{n_{\mathcal{N}_e}=1}^N \prod_{j=1}^{\mathcal{N}_v} \mathbb{E} [\alpha_j(\mathbf{n})] \quad (17) \end{aligned}$$

where $\mathbf{n} = (n_1, n_2, \dots, n_{\mathcal{N}_e})$, $\alpha_j(\mathbf{n}) = \prod_{n_i \in L_j} \alpha_j(n_i)$, and L_j is the index set of edges that are incident on vertex j . The incident index set L_j is called *paired*, when indexes are divided into partitions according to values, and each partition has an even number of elements. For example, $L_j = \{n_1, n_2, n_3, n_4, n_5, n_6\}$ is paired, when $n_1 = n_2$, and $n_3 = n_4 = n_5 = n_6$. Note that $\mathbb{E}[\alpha_j(\mathbf{n})] = 1$ if and only if the incident index set L_j is paired. Otherwise, $\mathbb{E}[\alpha_j(\mathbf{n})] = 0$.

Therefore, $E_\rho(G)$ can be obtained by counting the number of \mathbf{n} 's such that all L_j 's are paired, and dividing it by $N^{\mathcal{N}_e}$. All L_j 's are paired, if G is evenly decomposed into subgraphs, and all edge indexes within each subgraph are assigned the same value between 1 and N . This is equivalent to drawing vertices of the corresponding supergraph with N colors. Thus, the calculation of $E_\rho(G)$ is translated into counting the number of coloring methods for all supergraphs. We should, however, restrict adjacent vertices in each supergraph to be drawn with different colors, to avoid duplicated counting among supergraphs. Consequently, we have $E_\rho(G) = (1/N^{\mathcal{N}_e}) \sum_{k=1}^q P(S_k, N)$. ■



(a)



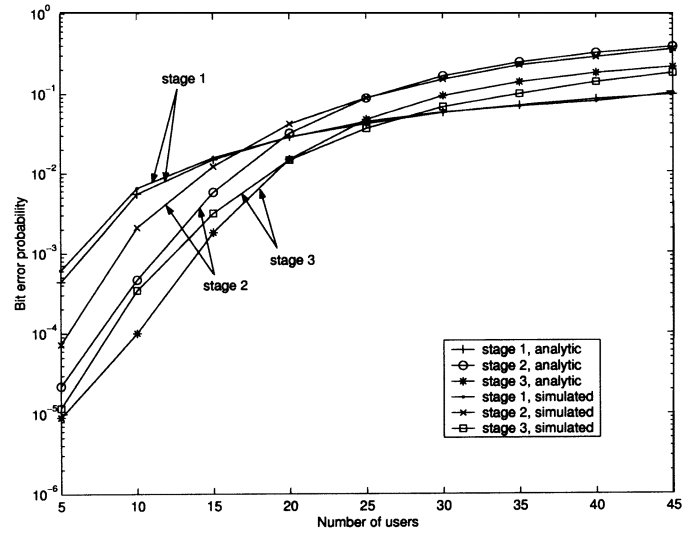
(b)

Fig. 6. Analytic and simulated results for normalized $E[Z_{p,1}^{(m)} | b_1 = 1]$ and $\text{Var}[Z_{p,1}^{(m)} | b_1 = 1]$ of the LPIC at the first to fifth stages when SNR = 10 dB for the desired user and $N = 31$. (a) $E[Z_{p,1}^{(m)} | b_1 = 1]$. (b) $\text{Var}[Z_{p,1}^{(m)} | b_1 = 1]$.

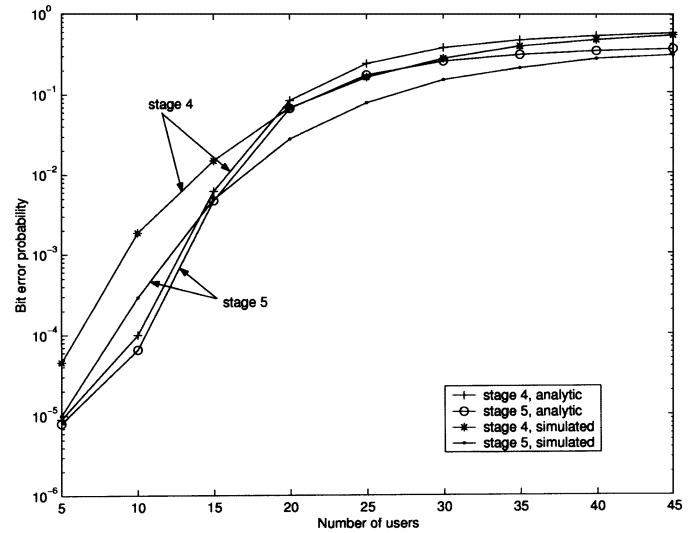
One more property shows that if graph G is disconnected by articulation points into p biconnected components G_1, \dots, G_p , then $E_\rho(G) = \prod_{i=1}^p E_\rho(G_i)$ and $E_\theta(G) = \prod_{i=1}^p E_\theta(G_i)$. The proposition and its proof can be found in [12].

Using these propositions, one can obtain $E_\theta(G_e)$ and $E_\rho(G_e)$ for an evolved graph G_e with tools in solving the Euler tour, the graph decomposition, the coloring, and the biconnected components finding problems. For example, let us compute $E_\rho(G)$ and $E_\theta(G)$ for the graph G in Fig. 5(a). The graph G in Fig. 5(a) can be divided into two biconnected components by an articulation point v_3 . Let G_1 and G_2 denote the upper and lower components, respectively. We have $E_\rho(G) = E_\rho(G_1)E_\rho(G_2)$ and $E_\theta(G) = E_\theta(G_1)E_\theta(G_2)$. Since G_1 is a simple cycle, $E_\theta(G_1) = 1/4$ and $E_\rho(G_1) = 1/N^2$ by Propositions 3 and 4.

Fig. 5(b) shows all even decompositions of G_2 , and Fig. 5(c) shows the corresponding supergraphs. By Proposition 4, $E_\rho(G_2) = (N + 3N(N - 1))/N^6 = 3/N^4 - 2/N^5$. There are



(a)



(b)

Fig. 7. Analytic and simulated results of the LPICs BEP for a different number of users with SNR = 10 dB for the desired user and $N = 31$. (a) From the first to the third stages. (b) From the fourth to the fifth stages.

six distinct Euler tours for G_2 . They are $(e_4, e_8, e_9, e_5, e_6, e_7)$, $(e_4, e_8, e_9, e_5, e_7, e_6)$, $(e_4, e_8, e_6, e_5, e_9, e_7)$, $(e_5, e_9, e_6, e_7, e_8, e_4)$, $(e_5, e_9, e_7, e_6, e_8, e_4)$ and $(e_6, e_8, e_4, e_7, e_9, e_5)$. By Proposition 3, $E_\theta(G_2) = 6/2^6 = 3/32$. As a result, $E_\rho(G) = E_\rho(G_1)E_\rho(G_2) = 3/N^6 - 2/N^7$, and $E_\theta(G) = E_\theta(G_1)E_\theta(G_2) = 3/128$. Without these propositions, it is difficult to directly compute $E_\rho(G) = E[\rho_{1,2}\rho_{2,3}\rho_{3,1}\rho_{3,4}\rho_{3,6}^2\rho_{4,6}\rho_{5,3}\rho_{6,5}]$ and $E_\theta(G) = E[\cos\theta_{1,2}\cos\theta_{2,3}\cos\theta_{3,1}\cos\theta_{3,4}\cos^2\theta_{3,6}\cos\theta_{4,6}\cos\theta_{5,3}\cos\theta_{6,5}]$.

VII. SIMULATION RESULTS

Numerical simulations were performed under an environment of synchronous transmission, coherent detection, random signature waveforms with $N = 31$ and the AWGN channel. The power levels for all users were fixed. To fully demonstrate the properties of LPIC and LSIC, we present two different power distributions for these two receivers.

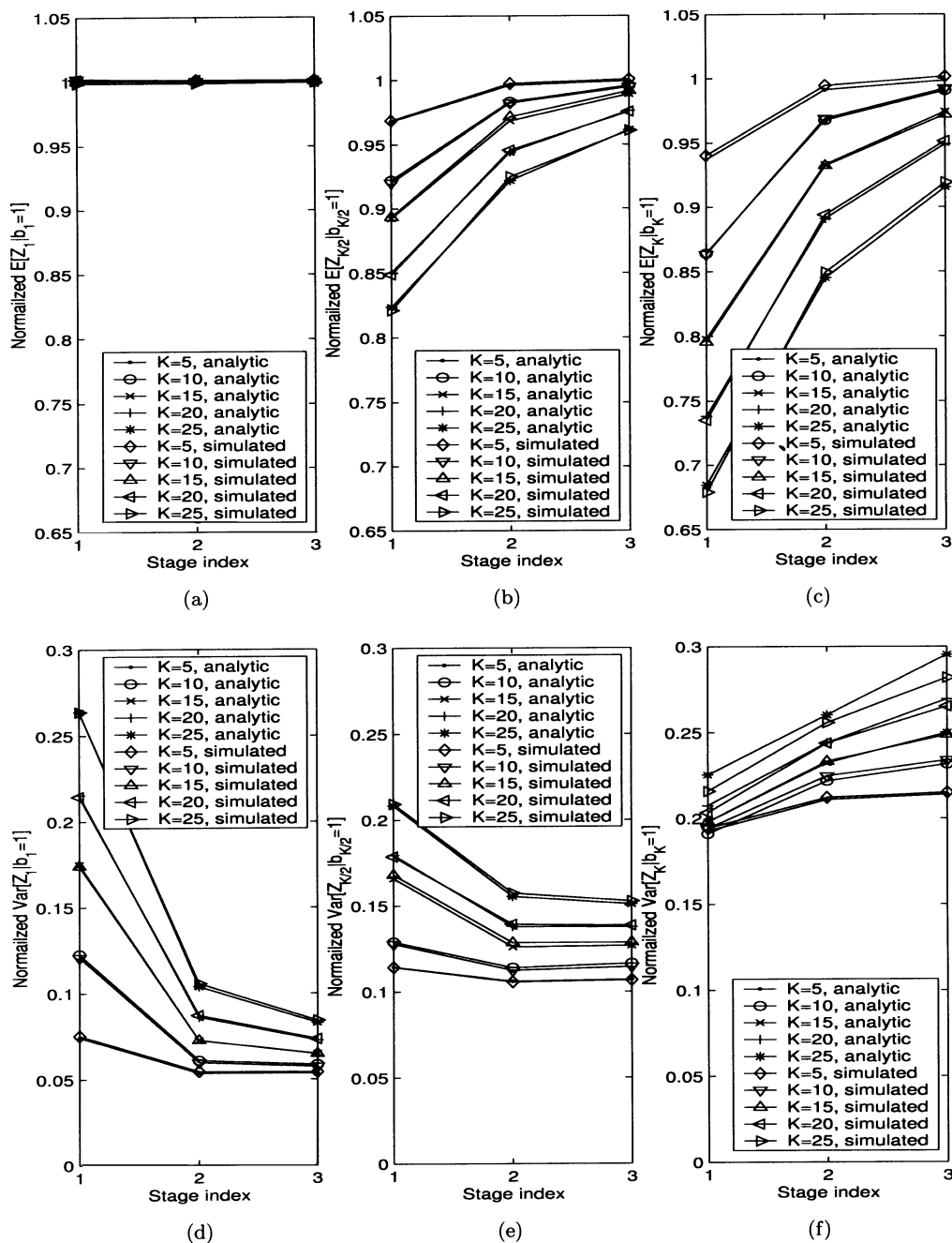


Fig. 8. Analytic and simulated results for normalized $E[Z_{s,k}^{(m)}|b_k = 1]$ and $\text{Var}[Z_{s,k}^{(m)}|b_k = 1]$ of the LSIC when SNR = 10 dB for the first user. (a) $E[Z_{s,1}^{(m)}|b_1 = 1]$ (the first user). (b) $E[Z_{s,1}^{(m)}|b_{\lfloor K/2 \rfloor + 1} = 1]$ (the middle user). (c) $E[Z_{s,K}^{(m)}|b_K = 1]$ (the last user). (d) $\text{Var}[Z_{s,1}^{(m)}|b_1 = 1]$. (e) $\text{Var}[Z_{s,1}^{(m)}|b_{\lfloor K/2 \rfloor + 1} = 1]$. (f) $\text{Var}[Z_{s,K}^{(m)}|b_K = 1]$.

A. LPIC

Since all users in LPIC were equivalent in the LPIC simulation, we chose user 1 as the desired user. In this environment, $K_1 = \lfloor K/2 \rfloor$ users had the same received energy per symbol as that of the desired user E_1 , and the remaining $K - K_1$ users had the energy level equal to $E_1/2$.

Fig. 6(a) compares analytic and simulated results for the normalized $E[Z_{p,1}^{(m)}|b_1 = 1]$ from the first to the fifth stages. In this test, the signal-to-AWGN-noise ratio (SNR) is equal to 10 dB for the desired user. The normalization is performed by dividing $E[Z_{p,1}^{(m)}|b_1 = 1]$ with a factor $\sqrt{E_1}$. It can be seen that analytic results match well with simulation results. As given in (5), the bias of $E[Z_{p,1}^{(m)}|b_1 = 1]$ from $E[Z_{p,1}^{(1)}|b_1 = 1]$ is negative when

the stage number is even, and positive when it is odd. The bias grows with the number K of users in the system. As analyzed in [6], the bias effect comes from the fact that the decision statistics of interferers (hence, the estimates of interfering signals) are correlated with the desired user's power and information bit. When these estimates are used to construct and remove the interference, the bias effect appears.

Fig. 6(b) compares analytic and simulated results for the normalized $\text{Var}[Z_{p,1}^{(m)}|b_1 = 1]$ from the first to the fifth stages. As before, SNR is equal to 10 dB for the desired user. The normalization is done with a factor E_1 . When the stage index is larger than two, the variance tends to increase as the stage index goes up, which indicates that interference cancellations at higher

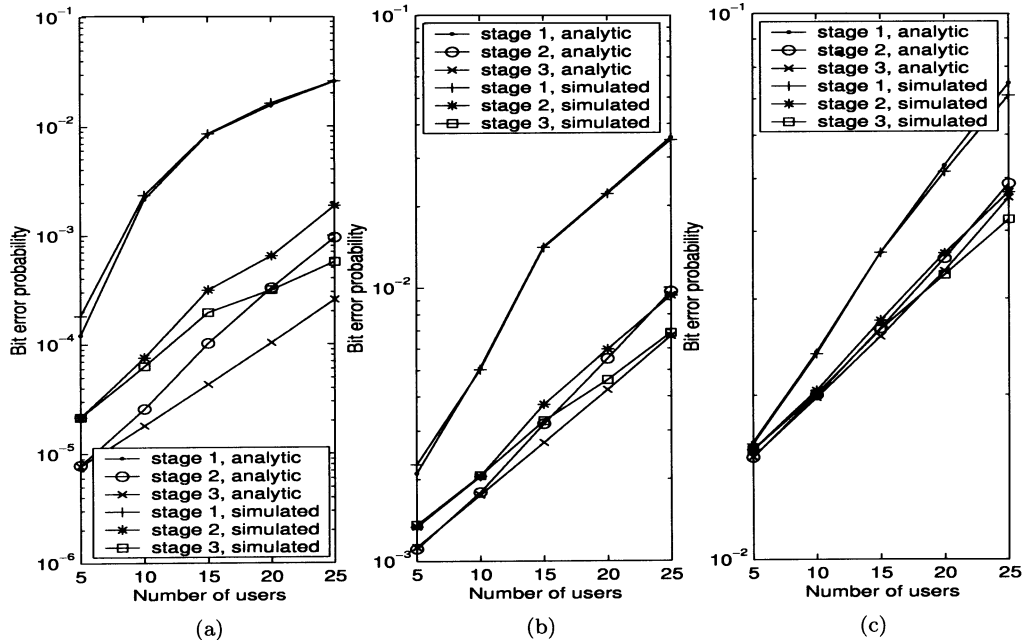


Fig. 9. Analytic and simulated results of the LSICs BEP from the first to third stages when $\text{SNR} = 10$ dB for the first user. (a) First user. (b) Middle user. (c) Last user.

stages are not effective when the number of users is larger than a threshold. The divergence effect occurs when the spectral radius of the matrix $(\mathbf{I} - \mathbf{R})$ in (1) is greater than one, which is very likely when random signature sequences are employed. The divergence effect of the PIC receiver has been experimentally investigated by researchers [16], which leads to the study of the partial PIC receivers [10], [17], [18]. In this paper, we give an exact analysis of the divergence effect. The analytical formulas for the mean and the variance of the decision statistics will be useful in the determination of partial cancellation factors in partial PIC receivers, which were found empirically or with adaptive methods [6], [10], [18].

In Fig. 7(a), we present analytic and simulated bit-error probability (BEP) performances from the first to the third stages with $\text{SNR} = 10$ dB. The analytic BEP is obtained using the method presented in [19, App. E], i.e., inserting the data of Fig. 6(a) and (b) into (3) and plugging into the $Q(\cdot)$ function. It can be seen that, when the stage index is larger than one, analytic and simulated BEPs do not match well if the number of users is less than 15. The discrepancy between simulated and analytic results is due to the breakdown of the central limit theorem (CLT). Although CLT proves the convergence of the decision statistic in distribution to a Gaussian function, the Gaussian assumption actually leads to inaccurate results, especially at low BEP. This was explained well in [1].

In Fig. 7(b), we show simulated and analytic BEP results at the fourth and fifth stages with $\text{SNR} = 10$ dB for the desired user. Compared with cases from $Z_{p,1}^{(1)}$ to $Z_{p,1}^{(3)}$, the results for $Z_{p,1}^{(4)}$ and $Z_{p,1}^{(5)}$ are less accurate. It is observed from Fig. 7(a) and (b) that the convergence speed is inversely proportional to the stage index. Also, based on (5), the user number should be constrained such that $1 - (-1)^m X(m)$ is larger than zero. Otherwise, the sign of the decision statistic is inverted from that of the actual data. This limit can be observed from the curve of the fourth stage in Fig. 7(b). If $K > 40$, $1 - X(4)$ is smaller than

zero, and the BEP at the fourth stage is almost 0.5, which leads to almost zero channel capacity.

It is also observed that the BEP performance depends mainly on the ratio K/N , which indicates that large-system results can be very useful in many cases of interest.

B. LSIC

Users were assigned with three different received energy levels E_1 , $E_1/2$, and $E_1/4$ in the simulation of the LSIC receiver. Since the LSIC receiver sorts users in a descending order according to their received powers, E_1 was assumed to be assigned to users 1 to $\lfloor K/3 \rfloor$; $E_1/2$ to users $\lfloor K/3 \rfloor + 1$ to $\lfloor 2K/3 \rfloor$; and $E_1/4$ to users $\lfloor 2K/3 \rfloor + 1$ to K . The BEP performances of the first, the middle ($(\lfloor K/2 \rfloor + 1)$ th), and the last (K th) users are analyzed and compared with experimental results.

Fig. 8(a)–(c) compare analytic and simulated results for the normalized $E[Z_{s,k}^{(m)} | b_k = 1]$, $k = 1, \lfloor K/2 \rfloor + 1, K$, at three stages. The SNR for the highest power users is set to 10 dB, and the normalization is done by a factor of $\sqrt{E_k}$. In this test, the second-order approximation, $(\mathbf{I} + \mathbf{L})^{-1} \approx \mathbf{I} - \mathbf{L} + \mathbf{L}^2$, is used for the detailed representation of \mathbf{M} when computing $X_{s,k}^{(m)}$. It is observed that analytic and simulated results match each other well.

Also, note that there is no bias effect for the conditional mean of the first user's decision statistic, while the conditional means for the medium and last users are negatively biased from 1. This can be seen from (8). Let us take Fig. 3(c) as an example. In all subrepresentations of $X(2, k)$, the out degree of vertex 1 is larger than 0. But, vertex 1 is constrained to be colored with the smallest color index 1 when computing $X_{s,1}^{(m)}$. Therefore, $X_{s,1}^{(m)} = 0$.

Fig. 8(d)–(f) compare analytic and simulated results for the normalized $\text{Var}[Z_{s,k}^{(m)} | b_k = 1]$, $k = 1, \lfloor K/2 \rfloor + 1, K$, at the first three stages when $\text{SNR} = 10$ dB for the first user. The second-order approximation is used for the inverse matrix $(\mathbf{I} + \mathbf{L})^{-1}$, if there are less than or equal to four arcs in the

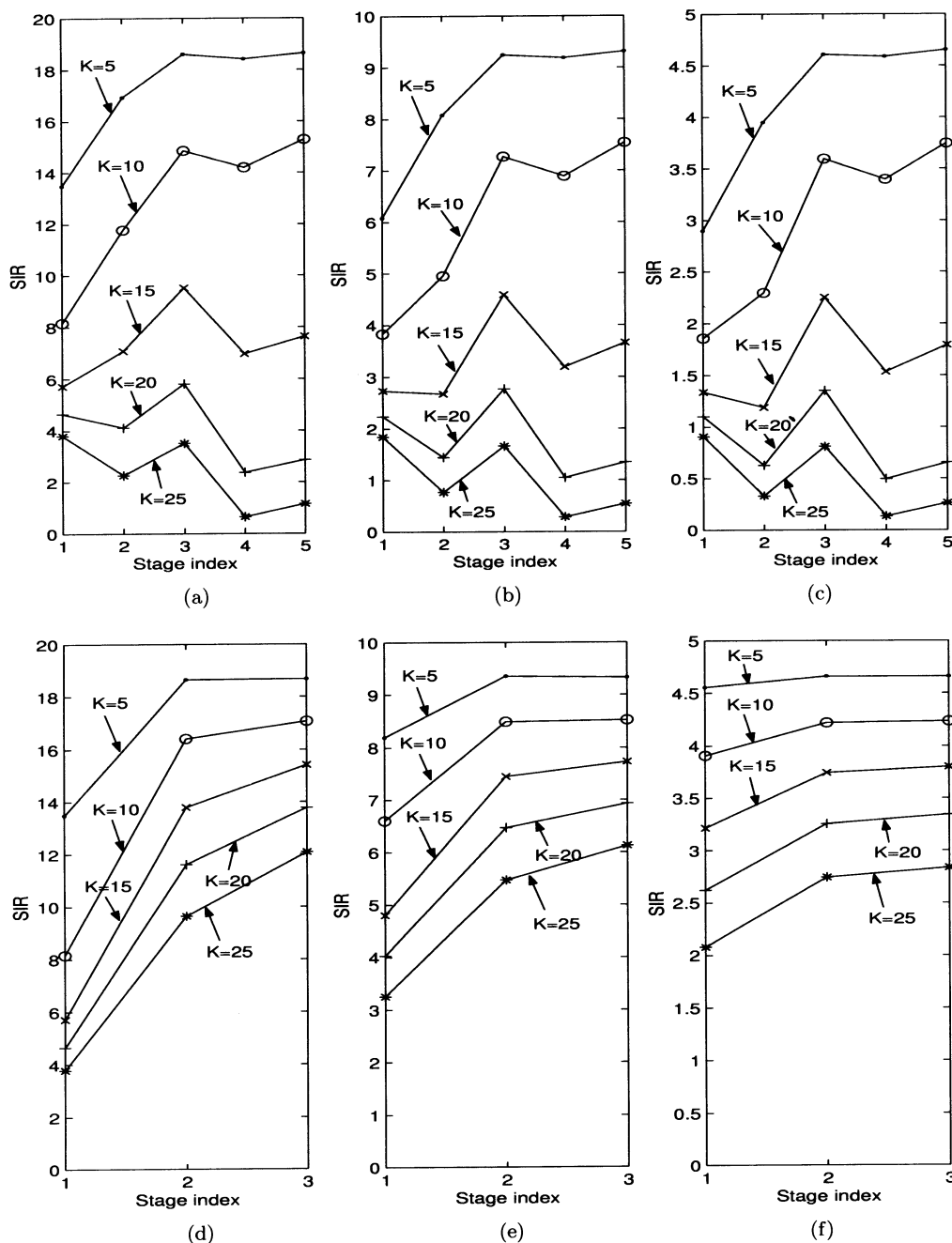


Fig. 10. SINR performance comparison of LPIC and LSIC receivers when $N = 31$ and $K = 5$ to 25. (a) First user of the LPIC. (b) Middle user of the LPIC. (c) Last user of the LPIC. (d) First user of the LSIC. (e) Middle user of the LSIC. (f) Last user of the LSIC.

macro representation. Otherwise, the first-order approximation that $(\mathbf{I} + \mathbf{L})^{-1} \approx (2\alpha - \alpha^2)\mathbf{I} - \alpha^2\mathbf{L}$ with α_{opt} listed in [12]. In this way, the total number of vertices is restricted to no greater than 12 to alleviate the computational complexity. The normalization is performed using the factor E_k . We see that, except for the cases of $K = 25$ in Fig. 8(f), analytic results match well with simulated ones. In this case, the discrepancy comes from the approximation error of the matrix inversion. Since only two or three rightmost paths are selected from K paths for the detailed representation, the discrepancy is proportional to the value of K . Moreover, because there are two arcs leaving vertex 1 in the complete representation of $Y_{s,k}^{(m)}$, the chromatic polynomial of $Y_{s,K}^{(m)}$ yields a larger value than those of $Y_{s,1}^{(m)}$ and $Y_{s,[K/2]+1}^{(m)}$. It follows that $Y_{s,K}^{(m)}$ has the largest approximation error.

In Fig. 9, we present analytic and simulated BEP results when $\text{SNR} = 10$ dB for the first user. It is seen that analytic and simulated BEP match well, except for the last user with $K = 25$, and the first user at the second and third stages. The former case is due to the inaccurate analytic result for $\text{Var}[Z_{s,K}^{(m)} | b_K = 1]$ when $K = 25$. The latter case can be explained in the same way as the LPIC receiver in Fig. 7. Moreover, the accuracy of the analytic BEP for the k th user at the m th stage depends on the convergence speed of $Z_{s,k}^{(m)}$. The convergence speed is inversely proportional to the stage index due to the structure complexity. Therefore, the accuracy of BEP at the first stage are better than those at the second and the third stages. Also, the number of terms within $Z_{s,1}^{(m)}$ is less than those in $Z_{s,[K/2]+1}^{(m)}$ and $Z_{s,K}^{(m)}$ for $m = 2, 3$. Hence, analytic BEP for the first user at stages

two and three are not so accurate as those for the middle and the last users, because a smaller number of terms results in slower convergence.

At last, the SINR performance of the LPIC and LSIC is compared. To conduct a fair comparison, the power assignment of the LPIC is set to be the same as that of the LSIC, i.e., three different received energy levels E_1 , $E_1/2$, and $E_1/4$ for users 1 to $\lfloor K/3 \rfloor$, $\lfloor K/3 \rfloor + 1$ to $\lfloor 2K/3 \rfloor$, and $\lfloor 2K/3 \rfloor + 1$ to K , respectively. It is shown in Fig. 10 that the SINR of the LSIC is no smaller than that of the LPIC for a user of the same stage index, which indicates, in a long-code CDMA, the LSIC outperforms the LPIC in terms of SINR. Moreover, the SINR curves of the LSIC increase with respect to the stage index, while those of the LPIC are in fluctuation.

VIII. CONCLUSION

The performance of the multistage LPIC and LSIC receivers in a synchronous long-code DS-CDMA system was analyzed in this paper. It was shown that the decision statistic is related to the moment of the matrix $(\mathbf{R} - \mathbf{I})$ for LPIC, and $(\mathbf{I} + \mathbf{L})^{-1}\mathbf{L}^T$ and $(\mathbf{I} + \mathbf{L})^{-1}$ for LSIC. We developed a graphical approach to facilitate the calculation of these moments, and showed that they can be obtained using tools arising from four well-known problems in graph theory, i.e., the coloring, the graph decomposition, the bi-connected component finding, and the Euler tour problems. Simulation results were performed to verify the correctness of our theoretical derivation of the mean and the variance of the decision statistic. With the Gaussian approximation, the estimated BEP performance was obtained by plugging the conditional mean and variance of decision statistics into the $Q(\cdot)$ function.

REFERENCES

- [1] S. Verdú, *Multuser Detection*. Cambridge, U.K.: Cambridge Univ. Press, 1998.
- [2] M. K. Varanasi and B. Aazhang, "Multistage detection in asynchronous code-division multiple-access communications," *IEEE Trans. Commun.*, vol. 38, pp. 509–519, Apr. 1990.
- [3] P. Patel and J. Holtzman, "Analysis of a simple successive interference cancellation scheme in a DS-CDMA system," *IEEE J. Select. Areas Commun.*, vol. 12, pp. 796–806, June 1994.
- [4] A. Kaul and B. D. Woerner, "Analytic limits on the performance of adaptive multistage interference cancellation," *Inst. Elect. Eng. Electron. Lett.*, vol. 30, no. 25, pp. 2093–2094, Dec. 1994.
- [5] A. L. C. Hui and K. B. Letaief, "Successive interference cancellation for multiuser asynchronous DS-CDMA detectors in multipath fading links," *IEEE Trans. Commun.*, vol. 46, pp. 384–391, Mar. 1998.
- [6] N. Correal, R. M. Buehrer, and B. D. Woerner, "A DSP-based DS-CDMA multiuser receiver based on partial interference cancellation," *IEEE J. Select. Areas Commun.*, vol. 17, pp. 613–630, Apr. 1999.
- [7] G. Xue, J. F. Weng, T. Le-Ngoc, and S. Tahar, "An analytical model for performance evaluation of parallel interference canceller in CDMA systems," *IEEE Commun. Lett.*, vol. 4, pp. 184–186, June 2000.
- [8] R. M. Buehrer, "Equal BER performance in linear successive interference cancellation for CDMA systems," *IEEE Trans. Commun.*, vol. 49, pp. 1250–1258, July 2001.
- [9] D. R. Brown, M. Motani, V. V. Veeravalli, H. V. Poor, and C. R. Johnson, "On the performance of linear parallel interference cancellation," *IEEE Trans. Inform. Theory*, vol. 47, pp. 1957–1970, July 2001.
- [10] D. Guo, L. K. Rasmussen, S. Sun, and T. J. Lim, "A matrix-algebraic approach to linear parallel interference cancellation in CDMA," *IEEE Trans. Commun.*, vol. 48, pp. 152–161, Jan. 2000.
- [11] L. K. Rasmussen, T. J. Lim, and A.-L. Johansson, "A matrix-algebraic approach to successive interference cancellation in CDMA," *IEEE Trans. Commun.*, vol. 48, pp. 145–151, Jan. 2000.
- [12] C.-H. Hwang, "Performance analysis of linear multistage interference cancellation in long-code CDMA systems," Ph.D. dissertation, Univ. Southern Calif., Los Angeles, CA, 2003.
- [13] D. B. West, *Introduction to Graph Theory*, 2nd ed. Englewood Cliffs, NJ: Prentice-Hall, 2000.
- [14] R. P. Stanley, "Acyclic orientations of graphs," *Discrete Math.*, vol. 5, no. 2, pp. 171–178, 1973.
- [15] Y. N. Sotskov, V. S. Tanaev, and F. Werner, *Scheduling Problems and Mixed Graph Colorings*. Magdeburg, Germany: Otto von Guericke Univ., 1998.
- [16] R. M. Buehrer, "On the convergence of multistage interference cancellation," in *Proc. Asilomar Conf. Signals, Systems, Computers*, vol. 1, 1999, pp. 634–638.
- [17] D. Divsalar, M. K. Simon, and D. Raphaeli, "Improved parallel interference cancellation for CDMA," *IEEE Trans. Commun.*, vol. 46, pp. 258–268, Feb. 1998.
- [18] G. Xue, J. Weng, T. Le-Ngoc, and S. Tahar, "Adaptive multistage parallel interference cancellation for CDMA," *IEEE J. Select. Areas Commun.*, vol. 17, pp. 1815–1827, Oct. 1999.
- [19] T. S. Rappaport, *Wireless Communications: Principles and Practice*, 2nd ed. Englewood Cliffs, NJ: Prentice-Hall, 2001.



Chien-Hwa Hwang (S'01) was born in Kaohsiung, Taiwan, in 1971. He received the B.S. and M.S. degrees from the National Taiwan University, Taipei, in 1993 and 1995, respectively, and the Ph.D. degree from the University of Southern California, Los Angeles, in 2003, all in electrical engineering.

In August 2003, he joined the Institute of Communications Engineering, National Tsing Hua University, Hsinchu, Taiwan, as an Assistant Professor. His research interests include multiuser detection, multi-carrier communications, and graph theory.



Chang-Su Kim (S'95–M'00) was born in Seoul, Korea, in 1971. He received the B.S. and M.S. degrees in control and instrumentation engineering in 1994 and 1996, respectively, and the Ph.D. degree in electrical engineering in 2000, all from Seoul National University (SNU), Seoul, Korea.

From 2000 to 2001, he was a Visiting Scholar with the Signal and Image Processing Institute, University of Southern California, Los Angeles, and a Consultant for InterVideo Inc., Los Angeles. From 2001 to 2003, he was a Postdoctoral Researcher with the School of Electrical Engineering, SNU. In August 2003, he joined the Department of Information Engineering, the Chinese University of Hong Kong, Hong Kong, as a Visiting Professor. His research topics include video and 3-D graphics processing and multimedia communications.



C.-C. Jay Kuo (S'83–M'86–SM'92–F'99) received the B.S. degree from National Taiwan University, Taipei, in 1980, and the M.S. and Ph.D. degrees from the Massachusetts Institute of Technology, Cambridge, in 1985 and 1987, respectively, all in electrical engineering.

He was Computational and Applied Mathematics (CAM) Research Assistant Professor in the Department of Mathematics at the University of California, Los Angeles, from October 1987 to December 1988. Since January 1989, he has been with the Department of Electrical Engineering-Systems and the Signal and Image Processing Institute at the University of Southern California, Los Angeles, where he currently has a joint appointment as Professor of Electrical Engineering and Mathematics. His research interests are in the areas of digital signal and image processing, audio and video coding, wavelet theory and applications, multimedia technologies, and large-scale scientific computing. He has authored around 500 technical publications in international conferences and journals.

Dr. Kuo is a member of SIAM, ACM, and a Fellow of SPIE. He is the Editor-in-Chief for the *Journal of Visual Communication and Image Representation*, Associate Editor for the IEEE TRANSACTIONS ON SPEECH AND AUDIO PROCESSING, and Editor for the *Journal of Information Science and Engineering*. He served as Associate Editor for the IEEE TRANSACTIONS ON IMAGE PROCESSING, 1995–1998, and the IEEE TRANSACTIONS ON CIRCUITS AND SYSTEMS FOR VIDEO TECHNOLOGY, 1995–1997. He received the National Science Foundation Young Investigator Award (NYI) and Presidential Faculty Fellow (PFF) Award in 1992 and 1993, respectively.